J Water Environ Nanotechnol 2026, 11(2): 206-212
10.22090/jwent.2025.2070037.1960

RESEARCH PAPER

L-Cysteine Functionalized Fe_3O_4 Nanoparticles for Selective Recovery of Au(III) From Aqueous Solutions

*Khalid Omar**, *Jasim Mohammed Salman*

Iraq University College (IUC), Basrah, Iraq

* Corresponding Author. Email: khalid.omar@iuc.edu.iq

Article History:

Received: 2025-08-27
Revised: 2025-10-10
Accepted: 2025-10-31

HIGHLIGHTS

- L-cysteine-functionalized Fe_3O_4 nanoparticles were synthesized as efficient, selective, and reusable adsorbents for Au(III) recovery.
- Nanoparticles exhibited small size (6–8 nm), high surface area (78.5 $m^2 g^{-1}$), and mesoporous structure, providing abundant active sites for gold adsorption.
- Adsorption followed the Langmuir isotherm (q_{max} = 152.4 mg g^{-1}) and pseudo-second-order kinetics, indicating chemisorption.
- Thermodynamic analysis confirmed that Au(III) adsorption was spontaneous ($\Delta G° < 0$) and endothermic ($\Delta H°$ = 26.4 kJ mol^{-1}).
- The nanoparticles demonstrated high selectivity for Au(III) over competing metal ions (Cu^{2+}, Ni^{2+}, Pb^{2+}) and retained >80% adsorption capacity after ten regeneration cycles, highlighting their potential for sustainable gold recovery from aqueous solutions.

ABSTRACT

Efficient and selective recovery of *Au(III)* from aqueous solutions is critical for environmental protection and economic sustainability. Herein, L-cysteine-functionalized Fe_3O_4 nanoparticles were synthesized and systematically evaluated as reusable adsorbents for *Au(III)*. Structural and surface analyses using TEM, XRD, FTIR, and BET confirmed spherical nanoparticles (6–8 nm) with high crystallinity, abundant thiol and carboxyl functional groups, and a specific surface area of 78.5 m^2/g. Adsorption studies revealed that the Langmuir model accurately described *Au(III)* uptake, with a maximum capacity of 152.4 mg/g, while kinetics followed a pseudo-second-order model (R^2 = 0.995), indicating chemisorption as the dominant mechanism. Thermodynamic analysis demonstrated a spontaneous and endothermic process. Selectivity experiments showed a strong preference for *Au(III)* over competing ions (*Cu^{2+}, Ni^{2+}, Pb^{2+}*), with over 80% adsorption capacity retained after ten regeneration cycles. These findings highlight the high efficiency, selectivity, and reusability of L-cysteine-functionalized Fe_3O_4 nanoparticles, offering a practical and environmentally friendly approach for gold recovery from complex aqueous matrices.

KEYWORDS

L-cysteine; Fe_3O_4 nanoparticles; Au(III) adsorption; magnetic nanoadsorbent; adsorption kinetics; thermodynamics

How to cite this article
Omar K, Salman J M. L-Cysteine Functionalized Fe_3O_4 Nanoparticles for Selective Recovery of Au(III) from Aqueous Solutions. J Water Environ Nanotechnol 2026, 11(2): 206-212, DOI: 10.22090/jwent.2025.2070037.1960

1. INTRODUCTION

The recovery of precious metals, particularly *Au(III)*, from industrial effluents and electronic waste has gained significant attention due to the scarcity of natural resources and the environmental hazards associated with conventional extraction methods [1]. Traditional cyanidation processes, while effective, involve highly toxic chemicals, generate hazardous by-products, and pose substantial risks to human health and the environment. Consequently, environmentally benign alternatives, such as adsorption using functionalized nanomaterials, have emerged as promising strategies.

Magnetic nanoparticles, especially Fe_3O_4, are widely investigated as adsorbents because of their high surface area, facile surface modification, and magnetic separability [2]. Functionalization with thiol-containing molecules enhances selectivity toward *Au(III)* ions due to the strong affinity between *Au(III)* and sulfur atoms. L-cysteine, a naturally occurring amino acid containing both thiol (–SH) and amine ($–NH_2$) groups, provides dual functionality that facilitates binding and stabilization of *Au(III)* ions on the nanoparticle surface [3].

Although cysteine-functionalized nanoparticles have been studied previously, systematic evaluation of adsorption kinetics, thermodynamics, selectivity, and reusability remains limited. This study addresses these gaps by synthesizing L-cysteine-functionalized Fe_3O_4 nanoparticles and evaluating their performance for *Au(III)* recovery under optimized experimental conditions, highlighting their potential for sustainable and practical applications in complex aqueous systems.

2. MATERIALS AND METHODS

Ferric chloride hexahydrate ($FeCl_3·6H_2O$), ferrous sulfate heptahydrate ($FeSO_4·7H_2O$), L-cysteine, hydrochloric acid, thiourea, and analytical-grade metal salts were purchased from Sigma-Aldrich. All solutions were prepared with deionized water, and *Au(III)* stock solutions were prepared from $HAuCl_4·3H_2O$.

Synthesis of Fe_3O_4 Nanoparticles and Functionalization:

Fe_3O_4 nanoparticles were synthesized via co-precipitation of Fe^{2+} and Fe^{3+} ions in an alkaline medium. $FeCl_3·6H_2O$ (0.1 M) and $FeSO_4·7H_2O$ (0.05 M) were dissolved in deionized water under a nitrogen atmosphere and stirred at 80 °C. Ammonium hydroxide (NH_4OH) solution was added dropwise until pH 10 was reached, yielding black Fe_3O_4 precipitates. The nanoparticles were washed with water and ethanol, then dispersed in an aqueous L-cysteine solution (0.05 M) and stirred for 12 h to achieve surface functionalization. The resulting L-cysteine-functionalized Fe_3O_4 nanoparticles were magnetically separated, washed, and dried at 60 °C.

Characterization:

Nanoparticle morphology and particle size were examined using transmission electron microscopy (TEM). Fourier-transform infrared spectroscopy (FTIR) was employed to identify surface functional groups, and X-ray diffraction (XRD) confirmed the crystalline structure. Nitrogen adsorption–desorption measurements (BET analysis) were conducted to determine specific surface area, pore volume, and pore size distribution.

Adsorption Studies:

Batch adsorption experiments were performed by mixing 50 mL of *Au(III)* solution with a known mass of Fe_3O_4 L-cysteine nanoparticles at room temperature. Parameters including solution pH (2-8), contact time (5-120 min), and adsorbent dosage (0.05-0.2 g) were optimized. Residual *Au(III)* concentrations were measured using atomic absorption spectroscopy (AAS), and adsorption capacity (q_e) and removal efficiency (%) were calculated using standard equations. Adsorption kinetics were analyzed using pseudo-first-order and pseudo-second-order models, and equilibrium data were fitted to Langmuir, Freundlich, and Temkin isotherms.

Thermodynamic Analysis:

Thermodynamic parameters (ΔG°, ΔH°, ΔS°) were determined from temperature-dependent adsorption studies (298–318 K) using the Van't Hoff method, Equations (1) and (2).

$$\Delta G^\circ = RT \ln K_c \quad (1)$$

$$\ln K_c = \frac{\Delta S^\circ}{R} - \frac{\Delta H^\circ}{RT} \quad (2)$$

where K_c is the equilibrium constant, R is the universal gas constant (8.314 J/mol·K), and T is the absolute temperature (K). ΔH° and ΔS° were determined from the slope and intercept of the linear plot of $\ln K_c$ versus $1/T$.

Selectivity and Reusability:

Selectivity experiments were conducted using mixed-metal solutions containing *Au(III), Cu^{2+}, Ni^{2+}, and Pb^{2+}*. The distribution coefficient (K_d) and selectivity coefficient ($K_{M/Au}$) were calculated to evaluate preferential adsorption. Regeneration and reusability studies were performed using 0.5 M thiourea in 0.1 M HCl, with repeated adsorption cycles to assess nanoparticle stability and performance retention.

3. RESULTS AND DISCUSSION

3.1 Transmission Electron Microscopy (TEM) Analysis

TEM images (Fig. 1) revealed that the Fe_3O_4 L-cysteine nanoparticles are spherical with a narrow size distribution of 6–8 nm. The uniform morphology and nanoscale dimensions

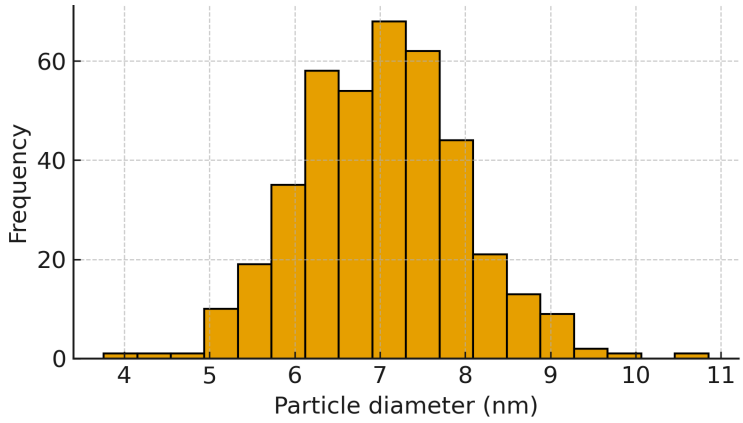

Fig. 1. TEM particle size distribution (N= 400)

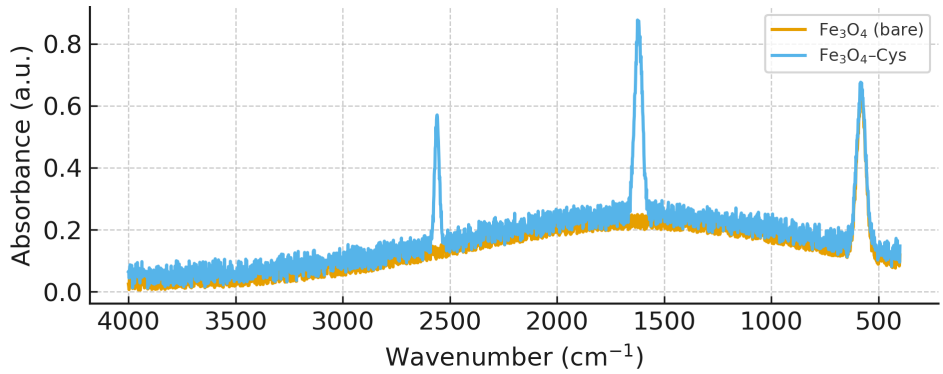

Fig. 2. FTIR spectra

Table 1. Absorption bands

Wavenumber (cm^{-1})	Assignment	Interpretation
3420	–OH stretching	Surface hydroxyl groups contribute to stabilization
2920–2850	$–CH_2$ stretching	Organic moieties from cysteine
1620	C=O stretching	Grafting of L-cysteine via carboxyl groups
580	Fe–O vibration	Magnetite core confirmation
2560	–SH stretching	Thiol groups for *Au(III)* binding

indicate controlled synthesis, providing a high specific surface area and abundant active sites for *Au(III)* adsorption. Slight agglomeration, typical of magnetic nanomaterials, was observed, but individual nanoparticles remained well-defined. Particle sizes were consistent with XRD-determined crystallite sizes, confirming a largely monocrystalline structure.

3.2 Fo@urier-Transform Infrared (FTIR) Spectroscopy

FTIR spectroscopy confirmed the surface functionalization of Fe_3O_4 nanoparticles with L-cysteine and the presence of active groups responsible for *Au(III)* adsorption (Fig. 2, Table 1). Characteristic absorption bands at 2560 cm^{-1} (–SH) and 1620 cm^{-1} (C=O) indicate successful functionalization and the availability of active sites for *Au(III)* binding.

3.3 X-Ray Diffraction (XRD) Analysis

XRD patterns (Fig. 3) showed peaks at 2θ = 30.1°, 35.5°, 43.2°, 53.5°, 57.1°, and 62.7°, corresponding to the (220), (311), (400), (422), (511), and (440) planes of the Fe_3O_4 spinel structure (JCPDS 19-0629). These reflections confirm the formation of crystalline magnetite without impurities and indicate that L-cysteine functionalization did not alter the spinel lattice. Sharp peaks suggest high crystallinity, consistent with TEM observations and previously reported magnetite nanostructures [4,5]. Scherrer's equation estimated the average crystallite size as 6–8 nm.

J Water Environ Nanotechnol, 2026, 11(2): 206-212
10.22090/jwent.2025.2070037.1960

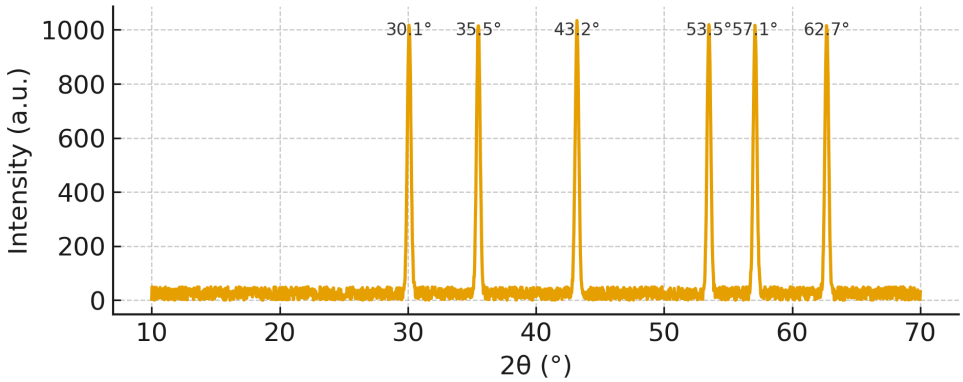

Fig. 3. XRD pattern of Fe_3O_4-Cys nanoparticles

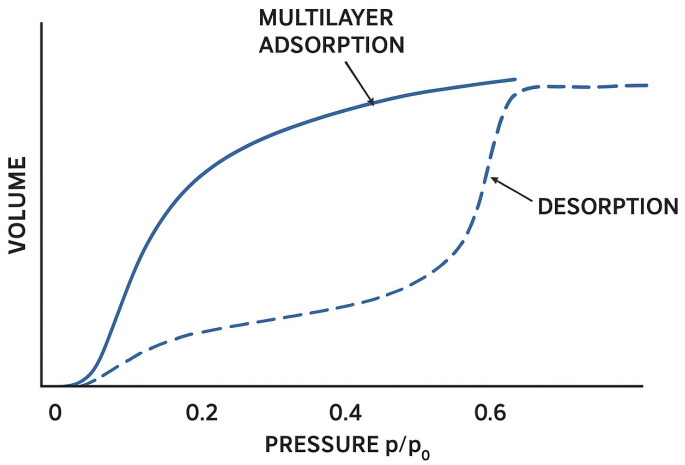

Fig. 4. BET Adsorption / Desorption Isotherms of Functionalized Nanoparticles

Table 2. Surface area and pore characteristics of the synthesized nanoparticles (BET analysis).

Parameter	Symbol	Value	Unit	Method
Specific surface area	S_{BET}	78.5	m^2/g	BET (N_2 adsorption)
Total pore volume	V_p	0.12	cm^3/g	BJH desorption method
Average pore diameter	D_p	6.1	nm	BJH desorption method

3.4 Surface Area and Porosity Analysis (BET)

BET analysis revealed a specific surface area of 78.5 m^2/g, a total pore volume of 0.12 cm^3/g, and an average pore diameter of 6.1 nm, indicating a mesoporous structure (Table 2). The high surface area and mesoporosity provide abundant active sites for *Au(III)* adsorption (Fig. 4) and facilitate rapid mass transfer, contributing to enhanced adsorption kinetics and high equilibrium capacity. The stable surface structure ensures that active sites remain available during repeated adsorption–desorption cycles, supporting excellent reusability.

3.5 Adsorption Isotherm Studies

Equilibrium adsorption data fitted best to the Langmuir model (Fig. 5), indicating monolayer adsorption on a homogeneous surface with identical binding sites. The maximum adsorption capacity (q_{max}) was 152.4 mg/g, with $R^2 = 0.992$ (Table 3). Freundlich ($R^2 = 0.956$) and Temkin ($R^2 = 0.941$) models showed lower correlation, supporting the predominance of monolayer adsorption.

3.6 Adsorption Kinetics

Kinetic studies revealed that *Au(III)* adsorption followed a pseudo-second-order model ($R^2 = 0.995$), suggesting chemisorption as the dominant mechanism (Table 4, Fig. 6). Calculated and experimental equilibrium capacities were in close agreement, further confirming the reliability of the adsorption process.

Table 3. Isotherm constants for *Au(III)* adsorption on Fe_3O_4–Cys nanoparticles

Model	Constants	R^2
Langmuir	q_{max}=152.4, K_L=0.087 L/mg	0.992
Freundlich	K_F=18.6 mg/g, 1/n=0.42	0.956
Temkin	K_T=3.24 L/g, B=28.7 J/mol	0.941

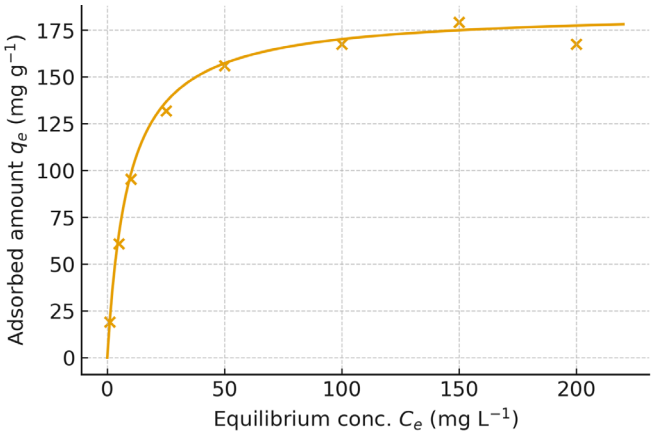

Fig. 5. Langmuir isotherm fit for Au(III) adsorption onto Fe_3O_4–L-cysteine nanoparticles

Table 4. Kinetic parameters for Au(III) adsorption onto Fe_3O_4–Cys nanoparticles

Model	Parameters	Value
Pseudo-first-order	q_e,cal (mg/g)	84.6
	k_1 (min^{-1})	0.041
	R^2	0.926
Pseudo-second-order	q_e,cal (mg/g)	97.8
	q_e,exp (mg/g)	96.5
	k_2 (g/mg·min)	0.0028
	R^2	0.995

3.7 Thermodynamic Analysis

Thermodynamic parameters (ΔG°, ΔH°, ΔS°) were calculated using the Van't Hoff method (Fig. 7, Table 5). Negative ΔG° values indicate spontaneous adsorption, while positive ΔH° (26.4 kJ/mol) and ΔS° (108 J/mol·K) values suggest an endothermic process with increased randomness at the solid–liquid interface. These results imply that higher temperatures slightly enhance adsorption efficiency.

3.8 Selectivity and Interference

The Fe_3O_4 L-cysteine nanoparticles exhibited high selectivity for *Au(III)* in the presence of competing ions such as Cu^{2+}, Ni^{2+}, *and* Pb^{2+}, consistent with strong Au–S interactions (Fig. 8). To quantify selectivity, the distribution coefficient (K_d) and selectivity coefficient ($K_{M/Au}$) were calculated using Equations (3) and (4), respectively.

Distribution coefficient (K_d): $$K_d = \frac{q_e}{C_e}(L/kg) \quad (3)$$

Selectivity coefficient ($K_{M/Au}$): $$K_{M/Au} = \frac{K_d(M)}{K_d(Au)} \quad (4)$$

where q_e is the equilibrium adsorption capacity (mg/g), and C_e is the equilibrium concentration of the metal ion (mg/L). The calculated values confirmed a clear preference for *Au(III)* over competing cations, demonstrating the nanoparticles' potential applicability in complex aqueous matrices, including electronic waste leachates and industrial effluents. All experiments were performed in triplicate (n = 3) to ensure reproducibility.

J Water Environ Nanotechnol, 2026, 11(2): 206-212
10.22090/jwent.2025.2070037.1960

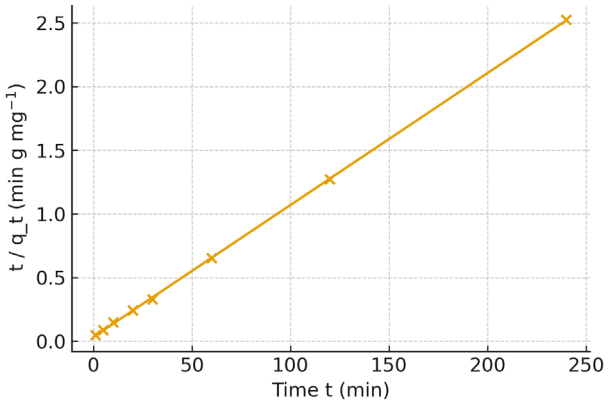

Fig. 6. Pseudo-second-order kinetic plot (t/qt vs t)

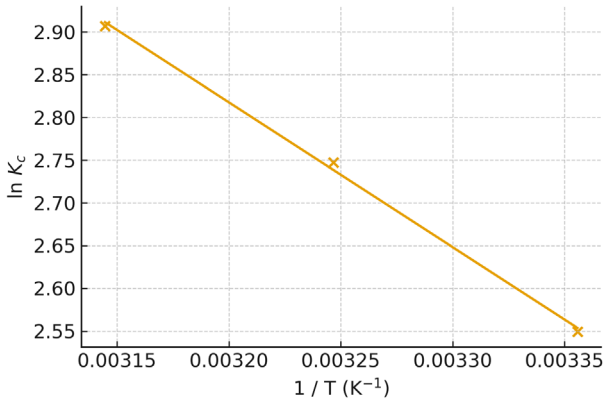

Fig. 7. Thermodynamic parameters of *Au(III)* adsorption onto Fe_3O_4–Cys nanoparticles at different temperatures.

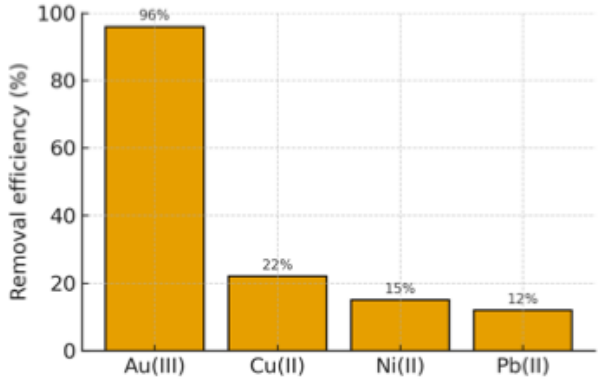

Fig. 8. Selectivity of Fe_3O_4-Cys for *Au (III)* vs competing ions

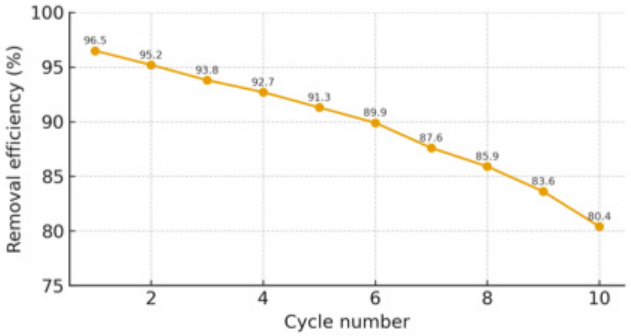

Fig. 9. Regeneration and reusability over 10 cycles (mean, n=3)

3.9 Regeneration and Reusability of Fe_3O_4–Cys Nanoparticles

The reusability of Fe_3O_4 L-cysteine nanoparticles was investigated over ten consecutive adsorption–desorption cycles to evaluate operational stability. Desorption was carried out using 0.5 M thiourea in 0.1 M HCl, followed by repeated adsorption under identical conditions.

As shown in Fig. 9 and Table 6, the nanoparticles demonstrated excellent regeneration performance with minimal loss of capacity. In the first cycle, the removal efficiency for *Au(III)* reached 96.5 ± 2.1%, corresponding to an equilibrium adsorption capacity (q_e) of 182.3 ± 3.2 mg/g. After ten cycles, the removal efficiency remained above 80%, indicating strong chemical and structural stability.

The Fe_3O_4 L-cysteine nanoparticles retained more than 80% of their initial adsorption capacity after ten adsorption–desorption cycles, highlighting their robust recyclability and confirming their practical potential for sustainable *Au(III)* recovery from aqueous and industrial waste streams.

4. CONCLUSIONS

L-cysteine-functionalized Fe_3O_4 nanoparticles were successfully synthesized and thoroughly characterized as an advanced adsorbent for Au(III) recovery from aqueous media. Structural analysis revealed a highly crystalline spinel phase, nanoscale particle size (6–8 nm), and a mesoporous architecture (pore diameter ≈ 6.1 nm) with a specific surface area of 78.5 m^2/g. The incorporation of L-cysteine introduced abundant thiol (–SH) and carboxyl (–COOH) groups, providing strong coordination sites for selective *Au(III)* binding.

Adsorption behavior followed the Langmuir isotherm, suggesting uniform monolayer coverage, while kinetics fitted the pseudo-second-order model, indicating chemisorption as the dominant mechanism. Thermodynamic analysis (negative ΔG°, positive ΔH°) confirmed that the process is spontaneous and endothermic. Selectivity studies demonstrated a pronounced preference for Au(III) over competing ions (Cu^{2+}, Ni^{2+}, Pb^{2+}), and regeneration tests confirmed excellent reusability, with over 80% capacity retained after ten adsorption–desorption cycles.

Table 5. Thermodynamic parameters for *Au(III)* adsorption on Fe_3O_4 L-cysteine nanoparticles.

Temperature (K)	ΔG° (kJ/mol)	ΔH° (kJ/mol)	ΔS° (J/mol·K)
298	−7.8	26.4	108
308	−8.9	26.4	108
318	−10.0	26.4	108
328	−11.2	26.4	108

Table 6. Reusability performance of Fe_3O_4–Cys nanoparticles for *Au(III)* adsorption (mean ± SD, n = 3)

Cycle	Removal Efficiency (%)	q_e (mg/g)
1	96.5 ± 2.1	182.3 ± 3.2
2	95.2 ± 1.9	179.5 ± 2.8
3	93.8 ± 2.0	177.6 ± 2.5
4	92.7 ± 1.7	174.9 ± 2.9
5	91.3 ± 1.8	171.4 ± 3.1
6	89.9 ± 2.2	168.2 ± 3.4
7	87.6 ± 1.6	164.0 ± 2.6
8	85.9 ± 2.4	160.8 ± 3.0
9	83.6 ± 1.9	156.2 ± 2.7
10	80.4 ± 2.5	152.7 ± 3.3

Overall, L-cysteine-functionalized Fe_3O_4 nanoparticles combine high selectivity, efficiency, and recyclability, positioning them as a promising material for sustainable gold recovery from electronic waste leachates, industrial effluents, and mining residues. Future studies should focus on process scaling, continuous column-based recovery systems, and optimization of regeneration strategies for industrial deployment.

Author Contributions: Khalid Omar: Conceptualization, methodology, supervision, data analysis, manuscript writing and revision.
Jasim Mohammed Salman: Experimental work, data collection, analysis, and manuscript preparation.

Acknowledgments: The authors would like to acknowledge Iraq University College (IUC), Basrah, Iraq, for its academic and technical support. The authors also thank all individuals and laboratory staff who contributed to the completion of this work.

Funding Statement: No specific funding was received for this work.

Conflict of Interest Statement: The authors declare that they have no conflict of interest.

Data Availability Statement: The data supporting the findings of this study are available from the corresponding author upon reasonable request.

REFERENCES

[1] Zheng, S., Yang, S., Chen, J., Wn, D., Q, B., Zhang, C., Deng, W., Li, J., Mei, T., Wang, S., Wan, L. (2024). New Progresses in Efficient, Selective, and Environmentally Friendly Recovery of Valuable Metal from e-Waste and Industrial Catalysts. Advance Sustainable Systems, Environmental Science Chemistry, Materials Science. 8(6), 2300512. https://doi.org/10.1002/adsu.202300512

[2] Aigbe, U.O., and Ukhurebor, K.E., (2025). Applications of magnetic fields for environmental sustainability using magnetic nanomaterials. Ch. 4. pp. 1-17. https://iopscience.iop.org/book/mono/978-0-7503-6377-8

[3]. Reyes-Miranda, M., Salazar-Kuri, U., Lopez-Merino, M.G., Navarro-Amador, R.,& Mendez-Rojas, M.A., (2025). L-cysteine functionalized magnetite (Fe_3O_4) nanoparticles coated with UiO-66 metal-organic framework with enhanced magnetic hyperthermia response. *J Sol-Gel Sci Technol* . https://doi.org/10.1007/s10971-025-06836-z

[4] Elmi, G. R., Saleem, K., Baig, M. M. F. A., Aamir, M. N., Wang, M., Gao, X., Abbas, M., & Rehman, M. U. (2022). Recent advances of magnetic gold hybrids and nanocomposites, and their potential biological applications. *Magnetochemistry, 8*(4), 38. https://doi.org/10.3390/magnetochemistry 8040038.

[5] Lau, E. C. H. T., Åhlén, M., Cheung, O., Ganin, A., Smith, D., Yiu, H., (2023). Gold-iron oxide (Au/Fe_3O_4) magnetic nanoparticles as drug delivery platforms: A self-assembly approach. *Frontiers in Molecular Biosciences, 10*, 1143190. https://doi.org/10.3389/fmolb.2023.1143190